PROCEEDINGS OF SPIE

SPIEDigitalLibrary.org/conference-proceedings-of-spie

Spiral amplifiers in a-Al₂ O₃:Er on a silicon chip with 20 dB internal net gain

S. A. Vázquez-Córdova, E. H. Bernhardi, Ke. Wörhoff, J. L. Herek, S. M. García-Blanco, et al.

SPIE.

Spiral amplifiers in a-Al_2O_3:Er on a silicon chip with 20 dB internal net gain

S. A. Vázquez-Córdova,[1,2] E. H. Bernhardi,[1] K. Wörhoff,[1] J. L. Herek,[2] S. M. García-Blanco,[1,2] and M. Pollnau[1,3]

[1]Integrated Optical MicroSystems Group, MESA+ Institute for Nanotechnology, University of Twente, P.O. Box 217, 7500 AE Enschede, The Netherlands

[2]Optical Sciences Group, MESA+ Institute for Nanotechnology, University of Twente, P.O. Box 217, 7500 AE Enschede, The Netherlands

[3]Department of Materials and Nano Physics, School of Information and Communication Technology, KTH - Royal Institute of Technology, Electrum 229, Isafjordsgatan 22-24, 16440 Kista, Sweden

ABSTRACT

Spiral-waveguide amplifiers in erbium-doped amorphous aluminum oxide are fabricated by RF reactive co-sputtering of 1-μm-thick layers onto a thermally-oxidized silicon wafer and chlorine-based reactive ion etching. The samples are overgrown by a SiO_2 cladding. Spirals with several lengths ranging from 13 cm to 42 cm and four different erbium concentrations between $0.5–3.0\times10^{20}$ cm^{-3} are experimentally characterized. A maximum internal net gain of 20 dB in the small-signal-gain regime is measured at the peak emission wavelength of 1532 nm for two sample configurations with waveguide lengths of 13 cm and 24 cm and erbium concentrations of 2×10^{20} cm^{-3} and 1×10^{20} cm^{-3}, respectively. The obtained gain improves previous results by van den Hoven *et al.* in this host material by a factor of 9. Gain saturation as a result of increasing signal power is investigated. Positive net gain is measured in the saturated-gain regime up to ~100 μW of signal power, but extension to the mW regime seems feasible. The experimental results are compared to a rate-equation model that takes into account migration-accelerated energy-transfer upconversion (ETU) and a fast quenching process affecting a fraction of the erbium ions. Without these two detrimental processes, several tens of dB/cm of internal net gain per unit length would be achievable. Whereas ETU limits the gain per unit length to 8 dB/cm, the fast quenching process further reduces it to 2 dB/cm. The fast quenching process strongly deteriorates the amplifier performance of the $Al_2O_3:Er^{3+}$ waveguide amplifiers. This effect is accentuated for concentrations higher than 2×10^{20} cm^{-3}.

Keywords: Amorphous aluminum oxide, erbium, optical gain, waveguide amplifier, spiral amplifier, rate-equation model.

1. INTRODUCTION

Rare-earth-doped materials have been of great interest because of their capability of optical amplification [1–5] and lasing [6,7]. In particular, erbium-doped materials offer a solution for signals around 1.53 μm in the telecommunication C-band [7]. In comparison with semiconductor optical amplifiers (SOAs) [8], rare-earth-doped optical amplifiers offer longer excited-state lifetimes [9], providing the capability for high-speed amplification [10] in the non-saturated-gain regime. Besides, a small gain dependence on temperature was demonstrated in different erbium-doped fibers [11,12] and waveguides [13]. Refractive index changes, usually observed in SOAs as a result of generating electron-hole pairs, are significantly weaker in rare-earth-doped materials [14]. Erbium-doped aluminum oxide ($Al_2O_3:Er^{3+}$) offers a broadband gain spectrum of 80 nm width [5], required for wavelength-division multiplexing (WDM). In addition, rare-earth-doped Al_2O_3 is easily deposited onto oxidized silicon substrates and patterned employing CMOS-compatible processes, facilitating its integration with different waveguide platforms including Silicon-on-Insulator (SOI) [15], polymer [16], and silicon nitride [17,18]. In our approach, a film of erbium-doped aluminum oxide is deposited onto oxidized silicon wafers by RF reactive co-sputtering from metallic targets in an oxygen atmosphere [3]. Low-loss channel waveguides

Integrated Optics: Devices, Materials, and Technologies XIX, edited by Jean-Emmanuel Broquin, Gualtiero Nunzi Conti, Proc. of SPIE Vol. 9365, 93650M · © 2015 SPIE
CCC code: 0277-786X/15/$18 · doi: 10.1117/12.2077503

are patterned via UV lithography in the $Al_2O_3:Er^{3+}$ layers, which are then processed by chlorine-based reactive ion etching [19] to define the waveguide channels.

Inhomogeneous linewidth broadening present in glass-doped materials decreases the transition cross-sections of rare-earth ions. Furthermore, energy-transfer up-conversion (ETU) among Er^{3+} ions and fast quenching processes [9,20,21] diminish the population inversion. Fast quenching processes arise from energy transfer to impurities, to host-material defects, or to neighboring clustered ions via static ETU [9,20,21]. In Al_2O_3, a fast quenching process limits the functional range of erbium doping concentrations for amplification [9]. As a consequence, the gain per unit length in $Al_2O_3:Er^{3+}$ is limited to a maximum of 2 dB/cm for a doping concentration of $\sim 2\times10^{20}$ cm^{-3} [5]. Channel waveguide amplifiers with lengths on the order of tens of centimeters are required to obtain substantial gain.

2. WAVEGUIDE DESIGN AND FABRICATION

Design considerations for an efficient waveguide amplifier require a geometrical waveguide cross-section that allows fundamental-mode operation at the pump and signal wavelengths. In addition, an overlap of both signal- and pump-mode fields with each other and with the active region is preferred, because it increases the interaction of the active ions in the waveguide with the signal-/pump-mode field. Decreasing the geometrical cross-section of the channel waveguide increases the intensity of the mode field [22], which serves two purposes, firstly, to tightly confine the mode field when non-straight waveguides are required and, secondly, to increase the pump intensity within the channel that, in principle, will result in higher pump absorption and, thus, higher population inversion and gain. As a consequence, lower pump powers will be needed to reach the gain threshold at the signal wavelength when comparing to the channel geometry applied in [5].

Since the $^4I_{11/2}$ lifetime is ~2 orders of magnitude smaller compared to the $^4I_{13/2}$ lifetime, a higher population density in the $^4I_{13/2}$ level is expected compared to the $^4I_{11/2}$ level. Consequently, following the results presented by Bradley *et al.* [5], the pump wavelength selected for the experiments was 976 nm instead of 1480 nm, because the stimulated emission on the $^4I_{13/2} \leftrightarrow {}^4I_{15/2}$ transition at the pump wavelength of 1480 nm plays a stronger role than at the $^4I_{11/2} \leftrightarrow {}^4I_{15/2}$ pump transition at 976 nm.

The Finite Difference (FD) algorithm in the Phoenix Field Designer software [23] was used to simulate the mode-field profile during the design of the waveguide cross-section, see Fig. 1(a), and the refractive indices were taken from [24]. The selected geometry consisted of a rib waveguide with a channel width of 1.5 μm and a channel height of 1 μm, with a ridge height of 0.35 μm. For this channel geometry, an overlap of ~95% and ~85% of the mode-field profile for the pump (λ = 976 nm) and signal (λ = 1532 nm), respectively, with the active region was determined. In Fig. 1(a) the signal-mode-field profile is shown over the waveguide cross section. Transverse-electric (TE) polarization was considered for the simulations and experiments.

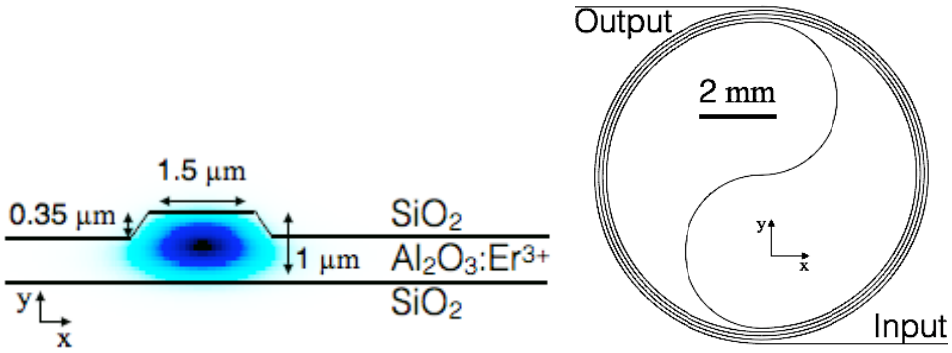

(a) (b)

Figure 1. (a) Geometrical cross-section of the channel waveguide, with the mode-field simulation at 1.53 μm superposed. (b) 13-cm-long spiral-waveguide design. (Figure taken from [13].)

Layers of Al_2O_3 doped with Er^{3+} were deposited onto oxidized silicon wafers using RF reactive co-sputtering [3]. UV lithography followed by chlorine-based reactive ion etching [19] was applied to pattern the waveguide channels on four Al_2O_3:Er^{3+} films with different doping concentrations of N_d = 0.45×10^{20}cm^{-3}, 0.95×10^{20}cm^{-3}, 1.92×10^{20}cm^{-3}, and 3.0×10^{20}cm^{-3}. A top-cladding layer of SiO_2 was deposited onto the active layer via PECVD. Unlike erbium-doped phosphate glasses [22,25], in Al_2O_3:Er^{3+} fast lifetime quenching was reported for doping concentrations above 3.0×10^{20} cm^{-3} [9], which governed our choice of lower doping concentration. To compensate for the low pump absorption at low doping concentrations and, consequently, lower inversion density, longer interaction distances between the pump and signal light and the active material were required. Spiral-shaped waveguides, see Fig. 1(b), were designed to minimize the footprint of the waveguide amplifiers on the wafer. Eight spirals of different length, from 12.9 cm to 41.6 cm, were patterned on each of the four samples with different Er^{3+} concentration. For the minimum bending radius of R = 2 mm bending losses of $<10^{-6}$ dB/cm were simulated. Losses at the center of the spiral due to the mode mismatch were estimated via simulations to be ~0.02 dB. Both losses are below the estimated propagation losses of ~0.1 dB/cm.

3. CHARACTERIZATION

Passive characterization of the waveguides was performed with a non-destructive method proposed by Okamura *et al.* [26]. A top-view image of the light scattered from a quarter of the spiral waveguide was captured using a InGaAs camera. An example image is shown in Fig. 2(a). A fiber-coupled diode-pumped neodymium laser (λ = 1320 nm) was applied as a light source. The waveguide propagation losses were determined by recording the scattered light intensity as a function of propagation length as shown in Fig. 2(b). The intensity of the scattered light is proportional to the intensity inside the channel, thus it is possible to correlate the scattered intensity as a function of propagation length with the Beer-Lambert law. The slope of the linear fit to the intensity distribution in semi-logarithmic scale determines the intensity decay rate in dB/cm. The lithographic mask was used to calibrate the spiral dimensions of the image. At λ = 1320 nm the propagation losses in the spiral waveguide are caused mainly by the material and fabrication defects, and the presence of Er^{3+} does not influence the background propagation loss measurements. Bradley *et al.* [5] found that the propagation losses, $\alpha_{abs}(\lambda)$, in Al_2O_3:Er^{3+} at 1530 nm and 980 nm were similar and ~0.18 dB/cm higher to the propagation losses at λ = 1320 nm. Background propagation losses in the spirals were determined to be, in average, 0.19±0.17 dB/cm.

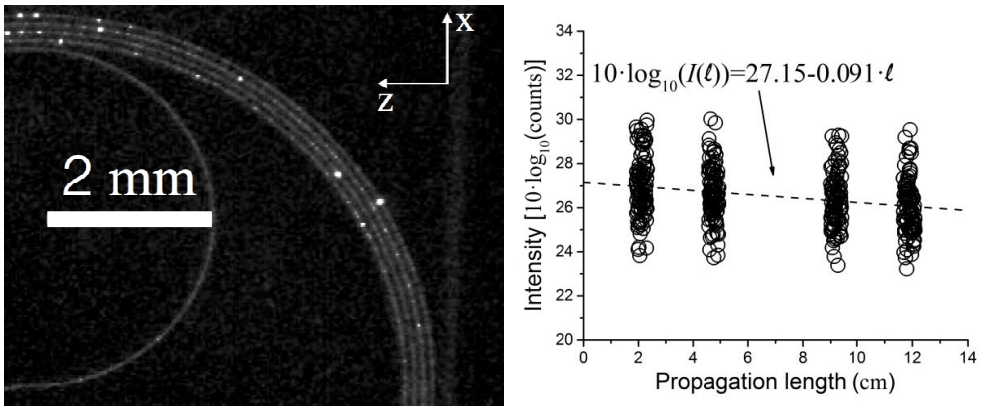

(a) (b)

Figure 2. (a) Infrared image of the scattered light at λ = 1.32 μm from a quarter of the spiral-shaped waveguide amplifier. (b) Intensity distribution in semi-logarithmic scale of the scattered infrared light along the propagation direction. Circles represent the measured intensity values, while the dashed line represents the linear fit to the data as a function of propagation length. (Figure taken from [13].)

For the gain characterization the pump-probe method was employed. The experimental setup consisted of a fiber-coupled diode (λ = 976 nm) serving as the pump, which was combined with the fiber-coupled signal laser (λ = 1532 nm) using a fiber-based WDM. The fiber output from the WDM was aligned to the input of the spiral waveguide. At the output end of the spiral waveguide a second fiber-based WDM was aligned to couple the output and separate the remaining pump from the amplified signal. The signal was modulated at 280 Hz, since lock-in amplification was required to discriminate the amplified signal from the amplified spontaneous emission. The signal intensity was measured with the pump source on, $I_{on}(\lambda)$, as well as with the pump source off, $I_{off}(\lambda)$. Then the gain was determined by the equation

$$G(\lambda) = 10\log_{10}\left(\frac{I_{on}(\lambda)}{I_{off}(\lambda)}\right) - \alpha_{abs}(\lambda)l - \alpha_{bck}(\lambda)l, \quad (1)$$

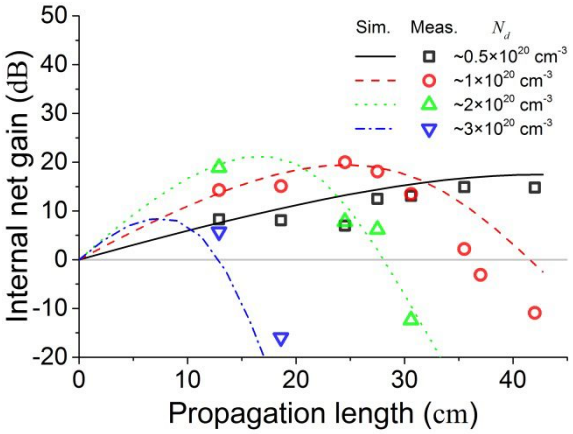

Figure 3. Internal net gain measured in $Al_2O_3:Er^{3+}$ spiral waveguides with different Er^{3+} concentrations (symbols) and simulated gain (lines) as a function of propagation length for different Er^{3+} concentrations. The rate-equation model presented in [9,13], which includes ETU and a fraction of fast-quenched ions, was used for the simulations.

where $\alpha_{abs}(\lambda)$ is the wavelength-dependent absorption coefficient of Er^{3+} in dB/cm, and ℓ is the spiral length. Figure 3 presents the small-signal gain measured in 21 spiral amplifiers of different lengths and Er^{3+} doping concentrations. The incident signal and pump powers were $P_s \sim 1$ μW and $P_p \sim 250$ mW, respectively. In average, 10% of the incident powers were coupled into the waveguide. From Fig. 3 one can observe that for low doping concentration lower gain is achieved due to low pump absorption and, thus, low inversion density. If the doping concentration significantly increases, the pump power available at the back part of the spiral waveguides is not enough to maintain the population inversion and, thus, the signal is reabsorbed, hence at longer spirals the gain drops. A maximum net gain of 20 dB was measured for two samples with lengths of 24.45 and 12.9 cm and doping concentrations of 0.95×10^{20} and 1.92×10^{20} cm^{-3}, respectively. The lines in Fig. 3 display the simulation results employing the quenched-ion model suggested by Agazzi *et al.* [9] and applied by the authors in [13]. From the simulation results, it is observed that the effect of fast quenching and ETU is accentuated at higher doping concentrations (3×10^{20} cm^{-3}), where less than 10 dB of total internal net gain was measured.

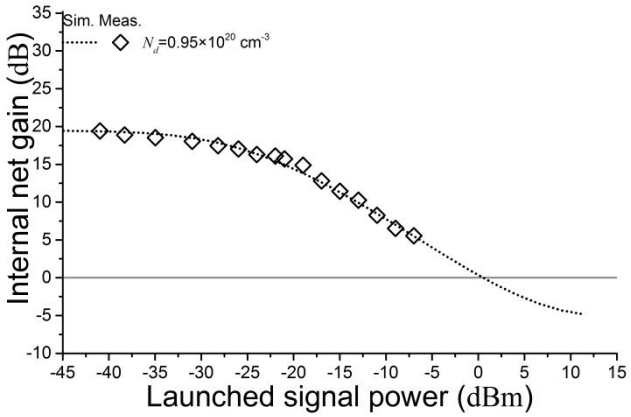

Figure 4. Maximum internal net gain at different signal powers, for a 24.45-cm-long spiral waveguide with a Er^{3+} concentration of 0.95×10^{20} cm^{-3}. Measurement results are presented by the symbols, while the line displays the simulation results using the rate-equation model presented in [13]. (Figure modified from [13].)

Gain saturation as a function of signal power was measured in a 25.45-cm-long spiral with $N_d = 0.95\times10^{20}$ cm^{-3}. The gain measurement and calculation were performed as previously described. The launched signal power was varied between –42 to –5 dBm, while the pump power remained constant as aforementioned. Gain saturation induced by increased signal power is presented in Fig. 4. When the signal power is increased, the stimulated emission of the signal at the beginning of the waveguide increases the population of Er^{3+} ions in the ground state. Since the pump power remains fixed, the Er^{3+} ions in the ground state at the beginning of the waveguide absorb more of the pump power available, reducing the pump power at the rear part of the waveguide, thus causing lower population inversion, more signal reabsorption and, therefore, lower gain. However, reasonable gain (>5 dB) was measured even in the strong saturated conditions and above 10 dB for launched signal powers lower than –15 dBm.

4. SUMMARY

The design of spiral amplifiers and their fabrication in $Al_2O_3:Er^{3+}$ have been demonstrated. Propagation losses in the spiral-shaped waveguides were determined and, in average, are 0.19 dB/cm. Experimental gain results of 21 spiral shaped amplifiers of different length and Er^{3+} doping concentration were presented. Gain was simulated with an advanced amplifier model [9,13] for the range of lengths and doping concentrations available for the samples, and results show good agreement with the experimental results. A maximum total gain of 20 dB was determined for two samples with lengths of 12.9 and 24.45 cm and doping concentrations of 0.95×10^{20} cm^{-3} and 1.92×10^{20} cm^{-3}, respectively. Gain saturation as a function of signal power was measured and simulated. 5.5 dB of net gain was measured in the saturated regime (-7dBm).

REFERENCES

[1] Geskus, D., Aravazhi, S., García-Blanco, S. M., and Pollnau, M., "Giant optical gain in a rare-earth-ion-doped microstructure," Adv. Mater. 24(10), OP19–OP22 (2012).

[2] Yang, J., Diemeer, M. B. J., Geskus, D., Sengo, G., Pollnau, M., and Driessen, A., "Neodymium-complex-doped photodefined polymer channel waveguide amplifiers," Opt. Lett. 34(4), 473–475 (2009).

[3] Wörhoff, K., Bradley, J. D. B., Ay, F., Geskus, D., Blauwendraat, T. P., and Pollnau, M., "Reliable low-cost fabrication of low-loss $Al_2O_3:Er^{3+}$ waveguides with 5.4-dB optical gain," IEEE J. Quantum Electron. 45(5), 454–461 (2009).

[4] Yang, J., van Dalfsen, K., Wörhoff, K., Ay, F., and Pollnau, M., "High-gain $Al_2O_3:Nd^{3+}$ channel waveguide amplifiers at 880 nm, 1060 nm, and 1330 nm," Appl. Phys. B 101(1–2), 119–127 (2010).

[5] Bradley, J. D. B., Agazzi, L., Geskus, D., Ay, F., Wörhoff, K., and Pollnau, M., "Gain bandwidth of 80 nm and 2 dB/cm peak gain in $Al_2O_3:Er^{3+}$ optical amplifiers on silicon," J. Opt. Soc. Am. B 27(2), 187–196 (2010).

[6] Bernhardi, E., van Wolferen, H., Agazzi, L., Khan, M., Roeloffzen, C., Worhoff, K., Pollnau, M., and de Ridder, R. M., "Ultra-narrow-linewidth, single-frequency distributed feedback waveguide laser in $Al_2O_3:Er^{3+}$ on silicon," Opt. Lett. 35(14), 2394–2396 (2010).

[7] Bradley, J. D. B., and Pollnau, M., "Erbium-doped integrated waveguide amplifiers and lasers," Laser Photonics Rev. 5(3), 368–403 (2011).

[8] Spiekman, L. H., "Semiconductor optical amplifiers" in [Optical Fiber Telecommunications Volume IVA], Kaminow, I. P., and Li, T., Eds., Academic Press, San Diego, CA, USA, 704 (2002).

[9] Agazzi, L., Wörhoff, K., and Pollnau, M., "Energy-transfer-upconversion models, their applicability and breakdown in the presence of spectroscopically distinct ion classes: A case study in amorphous $Al_2O_3:Er^{3+}$," J. Phys. Chem. C 117(13), 6759–6776 (2013).

[10] Bradley, J. D. B., Costa e Silva, M., Gay, M., Bramerie, L., Driessen, A., Wörhoff, K., Simon, J. C., and Pollnau, M., "170 GBit/s transmission in an erbium-doped waveguide amplifier on silicon," Opt. Express 17(24), 22201–22208 (2009).

[11] Kagi, N., Oyobe, A., and Nakamura, K., "Temperature dependence of the gain in erbium-doped fibers," J. Lightwave Technol. 9(2), 261–265 (1991).

[12] Suyama, M., Laming, R. I., and Payne, D. N., "Temperature dependent gain and noise characteristics of a 1480 nm-pumped erbium-doped fibre amplifier," Electron. Lett. 26(21), 1756–1758(1990).

[13] Vázquez-Córdova, S. A., Dijkstra, M., Bernhardi, E. H., Ay, F., Wörhoff, K., Herek, J. L., García-Blanco, S. M., and Pollnau, M., "Erbium-doped spiral amplifiers with 20 dB of net gain on silicon," Opt. Express 22(21), 25993–26004 (2014).
[14] Soulard, R., Zinoviev, A., Doualan, J. L., Ivakin, E., Antipov, O., and Moncorgé, R., "Detailed characterization of pump-induced refractive index changes observed in Nd:YVO_4, Nd:$GdVO_4$ and Nd:KGW," Opt. Express 18(2), 1553–1568 (2010).
[15] Agazzi, L., Bradley, J. D. B., Dijkstra, M., Ay, F., Roelkens, G., Baets, R., Wörhoff, K., and Pollnau, M., "Monolithic integration of erbium-doped amplifiers with silicon-on-insulator waveguides," Opt. Express 18(26), 27703–27711 (2010).
[16] Yang, J., Lamprecht, T., Wörhoff, K., Driessen, A., Horst, F., Offrein, B. J., Ay, F., and Pollnau, M., "Integrated optical backplane amplifier," IEEE J. Sel. Top. Quantum Electron. 17(3), 609–616 (2011).
[17] Belt, M., and Blumenthal, D. J., "Erbium-doped waveguide DBR and DFB laser arrays integrated within an ultra-low-loss Si_3N_4 platform," Opt. Express 22(9), 10655–10660 (2014).
[18] Hosseini, E. S., Purnawirman, Bradley, J. D. B., Sun, J., Leake, G., Adam, T. N., Coolbaugh, D. D., and Watts, M. R., "CMOS-compatible 75 mW erbium-doped distributed feedback laser," Opt. Lett. 39(11), 3106–3109 (2014).
[19] Bradley, J. D. B., Ay, F., Wörhoff, K., and Pollnau, M., "Fabrication of low-loss channel waveguides in Al_2O_3 and Y_2O_3 layers by inductively coupled plasma reactive ion etching," Appl. Phys. B 89(2–3), 311–318 (2007).
[20] Nilsson, J., Jaskorzynska, B., and Blixt, P., "Performance reduction and design modification of erbium-doped fiber amplifiers resulting from pair-induced quenching," IEEE Photonics Technol. Lett. 5(12), 1427–1429 (1993).
[21] Myslinski, P., Nguyen, D., and Chrostowski, J., "Effects of concentration on the performance of erbium-doped fiber amplifiers," J. Lightwave Technol. 15(1), 112–120 (1997).
[22] Patel, F. D., Dicarolis, S., Lum, P., Venkatesh, S., Member, S., and Miller, J. N., "A Compact High-Performance Optical Waveguide Amplifier," IEEE Photon. Technol. Lett. 16(12), 2607–2609 (2004).
[23] "Phoenix BV Software.", www.phoenixbv.nl.
[24] Bradley, J. D. B., [$Al_2O_3:Er^{3+}$ as a gain platform for integrated optics,] Ph.D. Thesis, University of Twente, Enschede, The Netherlands, 23 (2009).
[25] Yan, Y. C., Faber, A. J., de Waal, H., Kik, P. G., and Polman, A., "Erbium-doped phosphate glass waveguide on silicon with 4.1 dB/cm gain at 1.535 μm," Appl. Phys. Lett. 71(20), 2922–2924 (1997).
[26] Okamura, Y., Yoshinaka, S., and Yamamoto, S., "Measuring mode propagation losses of integrated optical waveguides: a simple method," Appl. Opt. 22(23), 3892–3894 (1983).